Original Research https://doi.org/10.5281/zenodo.21333921

Volume 8, Issue 1, pp 57-73, June 2026

ACHIEVERS JOURNAL OF SCIENTIFIC RESEARCH

Open Access Publications of Achievers University, Owo

Available Online at *www.achieversjournalofscience.org*

Synthesis, Spectroscopic Characterization, Mesogenic Properties and Thermal Studies of Six New Iridium(V) Long Carbon Chain Sulphate Chloride Complexes

F.S. Fabiyi[1*], O.D. Ogundele[1], M.A. Roja[2], I.V. Agunbiade[3], O.O. Oyebiyi[4], D.A. Oyegoke[1] and J.A. Lawal [1]

[1]Department of Chemical Sciences, Achievers University, Owo, Nigeria.
[2]Instituto de Quimica Fisica de los Materiales, Medio Ambiente y Energia, Universidad de Buenos Aires, Argentina.
[3]Department of Chemistry, University of Abuja, Abuja.
[4]Department of Biochemistry, Achievers University, Owo, Nigeria.

[*]**Corresponding author's Email**: fabiyi.fs@achievers.edu.ng

Submitted: March 3, 2026; **Revised**: May 20, 2026; **Accepted**: June 2, 2026; **Published**: June 30, 2026

Abstract

Six new iridium (V) complexes with long carbon chain sulphate chloride ligands, $[Ir(SDS)_2Cl_2]Cl$ (1), $[Ir(Myristyl\ sulphate)_2Cl_2]Cl$ (2), $[Ir(Cetyl\ sulphate)_2Cl_2]Cl$ (3), $[Ir(Stearyl\ sulphate)_2Cl_2]Cl$ (4), $[Ir(Arachidyl\ sulphate)_2Cl_2]Cl$ (5) and $[Ir(Behenyl\ sulphate)_2Cl_2]Cl$ (6), have been synthesized and characterized using various techniques, including IR, NMR, and mass spectrometry. The IR and NMR spectra confirmed the presence of alkyl sulphate and chloride ligands, while electronic absorption spectra and ionic conductivity revealed a low-spin d^5 configuration for the Ir(V) complexes. Thermal analysis revealed that the complexes exhibit liquid crystal properties, with melting points and decomposition temperatures increasing with alkyl chain length. The complexes showed ionic conductivity, with conductivity values ranging from 13.67 to 18.68 Ω^{-1} cm^2 mol^{-1}, indicating 1:1 electrolyte behaviour. Magnetic moment measurements confirmed a low-spin state for Ir^{5+}. The complexes' thermal stability increased with alkyl chain length, with decomposition temperatures ranging from 250 °C to 300 °C. This study highlights the potential of these iridium(V) complexes in applications such as optoelectronics and catalysis, and demonstrates the importance of alkyl chain length in determining their thermal properties.

Keywords: Iridium(V) complexes, liquid crystals, thermal analysis, spectroscopic characterization, alkyl sulphate ligands.

1.0 Introduction

In modern inorganic and materials chemistry research development, the important role of transition metal complexes continues to take the forefront. This is as a result of their structural diversity and tunable physicochemical properties (Housecroft & Sharpe, 2018). Owing to their diverse structural attributes and widespread utility in catalysis, materials science, and medicinal chemistry, transition metal complexes have generated considerable interest (Crabtree, 2019). Iridium complexes among them are especially interesting due to their excellent chemical stability, variable oxidation states and special electronic properties, which allow these compounds to be used in homogeneous catalysis, photochemistry and anticancer drugs (You & Nam, 2012). Iridium complexes attract attention due to their stable high oxidation states, strong spin–orbit coupling, and tunable photophysical behaviour (Lowry & Bernhard, 2006).

Recent studies have revealed that iridium complexes exhibit high photostability, strong spin–orbit coupling, modifyable emission properties, long-lived excited states and some with metallomesogenic properties, which make them suitable candidates in catalysis, sensing, optoelectronics, and biomedical applications (Zhao *et al*., 2011; Fan *et al*., 2018). Metallomesogenic systems have been extensively studied with metals such as copper, palladium, and platinum (Giroud-Godquin & Maitlis, 1991). However, reports on some transition-metal-based liquid crystalline materials remain comparatively limited, particularly for heavy transition metals like iridium (Donni *et al*., 2003). Studies have revealed that the formation of liquid crystalline phases in coordination compounds is strongly influenced by the presence of anisotropic, flexible, and amphiphilic ligands (Binnemans, 2005). Long alkyl chains play a critical role in promoting self-assembly, enhancing van der Waals interactions and inducing mesophase formation (Bruce, 2000).

Sodium dodecyl sulphate (SDS) and its higher homologues, ligands based on long-chain sulphate esters (18–24), form an important class of amphiphilic compounds (Rosen & Kunjappu, 2012). Unlike typical surfactants, the ligands here combine hydrophilic sulphate head groups and hydrophobic alkyl chains. The metal coordination of such ligands to transition metals can yield complexes that possess interesting physicochemical properties (Neumann *et al*., 2010). Members of this class of ligands have a polar sulphate head group ($–OSO_3^-$) and hydrophobic alkyl tail (C_{12}--C_{24}). These types of amphiphilic systems are well-known for their ability to form organized assemblies such as micelles, bilayers, and liquid crystalline phases (Binnemans, 2009). However, their coordination to transition metals, particularly iridium, remains understudied.

Lately, there have been increasing efforts in incorporating long-chain alkyl sulphates as ligands on metal complexes so as to investigate the effect of chain length on their structural, spectral and functional properties (Date *et al*., 2025). Despite these advances, there remains a significant gap in the exploration of long-chain amphiphilic ligand systems coordinated to iridium centres, especially in relation to their liquid crystalline behaviour (Donni *et al*., 2023).

Therefore, the studies is a bold step in which some new iridium-based complexes with long carbon chain sulphate ligands are synthesized, characterized and their thermal stability and phase transitions investigated. Chain lengths C_{24} to C_{40} were selected to span from typical surfactant range to extended hydrophobic tails, allowing systematic study of van der Waals effects on mesophase formation without introducing excessive steric hindrance.

2.0 Materials and Methods

2.1 Materials

All chemicals used were of AnalaR grade and were used without any further purification. The chemicals and solvents were sourced from Aldrich. The water used was doubly distilled and deionized.

2.2 Physico-chemical Measurements
The solubilities of each complex were tested in six different solvents: water, ethanol, acetone, dichloromethane, diethyl ether, and hexane.
To measure the pH of the complex solutions, a Mettler Toledo pH meter was used.

2.3 Conductivity Tests
Conductivity tests were carried out on the compounds: $C_{24}H_{48}IrCl_3O_8S_2$ ([Ir(SDS)$_2$Cl$_2$]Cl), $C_{28}H_{60}IrCl_3O_8S_2$ ([Ir(Myristyl sulphate)$_2$Cl$_2$]Cl), $C_{32}H_{68}IrCl_3O_8S_2$ ([Ir(Cetyl sulphate)$_2$Cl$_2$]Cl), $C_{36}H_{76}IrCl_3O_8S_2$ ([Ir(Stearyl sulphate)$_2$Cl$_2$]Cl) and $C_{40}H_{84}IrCl_3O_8S_2$ ([Ir(Behenyl sulphate)$_2$Cl$_2$]Cl). The solutions were prepared using doubly distilled deionized water and the conductivity of 10^{-3} M solutions at 25 °C using a Mettler Toledo Seven Excellence Conductivity Meter were determined.
To determine the magnetic moments of the complexes, a Sherwood Scientific Magnetic Susceptibility Balance (MSB) was utilized.

2.4 Elemental Analysis (CHN)
Elemental analyses (CHN) were carried out using a PerkinElmer 2400 Series II CHNS/O Analyzer.

2.5 Infrared Spectroscopy (IR)
For the Infrared Spectroscopy, we used a Shimadzu IRPrestige-21 FTIR Spectrometer. The IR spectroscopy was conducted over a wavelength range of 4000 – 400 cm^{-1} with a resolution of 4 cm^{-1}.

2.6 Nuclear Magnetic Resonance (NMR)
The Nuclear Magnetic Resonance (NMR) Spectroscopy was carried out on a Bruker Avance III 500 MHz NMR Spectrometer, using $CDCl_3$ as the solvent at a temperature of 25 °C and a spectral width of 0 – 10 ppm.

2.7 Mass Spectrometric Measurement
Waters Xevo G2-S Q-TOF Mass Spectrometer was used to conduct our mass spectrometry measurements at mass range of m/z 50 - 2000, with ethanol serving as the solvent.
The differential scanning calorimetry
The differential scanning calorimetry (DSC) studies were performed using the TA Instruments Q2000 DSC, covering a temperature range of 30 – 300 ^oC, with heating and cooling rates set at 10 ^oC/min.

2.8 Thermogravimetry and Polarized Optical Microscopy (POM) Analyses
The thermogravimetry and polarized optical microscopy (POM) analyses were carried out using the TA Instruments Q500 TGA and the Olympus BX53 Polarizing Microscope. The TGA was conducted between 30 – 600 ^oC at a heating rate of 5 ^oC/min, while for POM, we maintained a temperature range of 30 - 250 ^oC with the same heating rate of 5 ^oC/min.

2.9 Syntheses
2.9.1 [Ir(SDS)$_2$Cl$_2$]Cl
To prepare [Ir(SDS)$_2$Cl$_2$]Cl, 2.46 g of $IrCl_5$ (0.086 M) were dissolved in 25 mL of ethanol, stirring for about 15 minutes until it fully dissolved. This was followed by the addition of 20 cm^3 of 0.02 M SDS, the mixture was gently stirred, and then transferred it to a thermostatted water bath, heating it to 55 ^oC for 6 hours. Afterward, the reaction mixture was left to cool to room temperature. The resulting precipitate was filtered out, washed with doubly distilled

deionized water, recrystallized, and then dried in a desiccator for 48 hours. Purity was confirmed by CHN analysis within ±0.4% of calculated values, and by single melting point determination. Recrystallization was repeated until constant melting point was obtained. This was carried for all synthesis.

2.9.2 Ir(Myristyl sulphate)$_2$Cl$_2$]Cl

3.62 g (0.245 M) of $IrCl_5 \cdot 3H_20$ and 0.545.g, (2.0 mmol.) of sodium myristyl sulphate each dissolved in 10 mL of 1.5 mmol of ethanol were mixed together, stirred continuously for about 4 hrs to dissolve the $IrCl_5$. 1.50 mL of concentrated HCl was then added to the reaction mixture and stirred from another 2 hrs at room temperature. A precipitate was formed, and was concentrated under reduced pressure, and then, filtered off. The resulting precipitate was washed with doubly distilled deionized water, and recrystalised and dried on a desiccator for 60 hrs.

2.9.3 Ir(Cetyl sulphate)$_2$Cl$_2$]Cl

3.84 g (0.380 g, 0.1 M) of $IrCl_5 \cdot 3H_20$ and 0.650 g, (1.24 mmol.) of sodium cetyl sulphate each dissolved in 10 mL of 1.5 mmol of ethanol were mixed together, stirred continuously for about 4 hrs to dissolve the $IrCl_5$. 1.50 mL of concentrated HCl was then added to the reaction mixture and stirred from another 2 hrs at room temperature. A precipitate was formed, and was concentrated under reduced pressure, and then, filtered off. The resulting precipitate was washed with doubly distilled deionized water, and recrystalised and dried on a desiccator for 60 hrs.

Ir(Stearyl sulphate)$_2$Cl$_2$]Cl, Ir(Arachidyl sulphate)$_2$Cl$_2$]Cl and Ir(Behenyl sulphate)$_2$Cl$_2$]Cl were prepared as described above using the following reactants concentrations: for Ir(Stearyl sulphate)$_2$Cl$_2$]Cl, $IrCl_5 \cdot 3H_20$ (0.450 g, 0.1 M) and 0.66 g, (1.3.5 mol.) of sodium stearyl sulphate; for [Ir(Arachidyl sulphate)$_2$Cl$_2$]Cl, $IrCl_5 \cdot 3H_20$ (0.420 g, 0.15 M) and 0.550 g, (1.32 mol.) of sodium arachidyl sulphate; for Ir(Behenyl sulphate)$_2$Cl$_2$]Cl, $IrCl_5 \cdot 3H_20$ (0.460 g, 0.1 M) and 0.450 g, 1.34 mol of sodium Behenyl sulphate.

3.0 Results and Discussion

All the complexes are soluble in water and ethanol, which points to their ionic nature, and they show partial solubility in acetone. On the other hand, none of them dissolved in dichloromethane, diethyl ether, or hexane. These solubility tests suggest that the complexes possess ionic and polar characteristics, making them soluble in polar solvents like water and ethanol (Shriver & Atkins, 2010).

The conductivity values range from 13.67 to 18.68 Ω^{-1} cm^2 mol^{-1}, indicating that these compounds are indeed ionic. They likely behave as 1:1 electrolytes, producing one cation $[Ir(L)_2Cl_2]^+$ and one anion Cl^-, where L represents the ligands (Geary, 1971). The conductivity readings suggest that these compounds are ionic but act as weak electrolytes due to the presence of large cations. The magnetic moments of the complexes were measured and found to be in the range, μ = 4.34 to 4.80 BM. This is within the range of magnetic moment susceptibility expected for low spin octahedral d^4 complexes (Figgis & Hitchman, 2000). This suggests that Ir^{5+} in these complexes are in a low-spin state, consistent with Ir(V) in an octahedral field with strong-field ligands (Lever, 1984).

The molecular weights of the complexes range from 871.48 to 1172.10. The results from the physical measurements conducted on the complexes in Table 1.

Table 1. Physicochemical and magnetic data for complexes 1-6

Empirical formula (formula weight)	Colour	Yield (%)	M. Pt (°C)	Analysis % found (calculated) S	C	H	O	μeff. λ m (BM}	(Ω^{-1} cm^2 mol^{-1})
$C_{24}H_{48}IrCl_3O_8S_2$ (807.17)	Yellow	63.65	117 -118	6.55	29.45	4.95	13.10	4.34	98.26
$C_{28}H_{60}IrCl_3O_8S_2$ (887,52)	Pale yellow	58.24	129 -131	6.05	40.70	7.20	12.06	4.42	93.72
$C_{32}H_{68}IrCl_3O_8S_2$ (943.63)	Cream	56.32	135 -136	5.20	46.85	8.05	10.40	4.58	91.22
$C_{36}H_{76}IrCl_3O_8S_2$ (999.63)	Off-White	62.12	153	5.20	46.85	8.05	10.40	4.62	90.34
$C_{40}H_{84}IrCl_3O_8S_2$ (1055.92)	White	56.26	159 -161	4.85	49.45	8.40	9.70	4.73	89.46
$C_{44}H_{92}IrCl_3O_8S_2$ (1111.84)	White	59.44	170 -172	4.55	51.80	8.70	9.15	4.80	87.32

3.1 IR Spectrum

The IR spectrum of the complexes displays numerous peaks between 4000 and 400 cm^{-1}, which have been carefully assigned as shown in Table 2 (Nakamoto, 2009). For instance, the IR spectrum of $[Ir(SDS)_2Cl_2]Cl$ reveals peaks that indicate the presence of various functional groups in the compound. The peaks at 2924 and 2853 cm^{-1} correspond to the asymmetric and symmetric stretching vibrations of the CH_2 groups, respectively, while the peak at 1467 cm^{-1} is linked to the bending vibration of the CH_2 groups (Silverstein *et al*., 2014).

Additionally, the peaks at 1215 and 1068 cm^{-1} are associated with the asymmetric and symmetric stretching vibrations of the SO_4 groups, respectively (Nakamoto, 2009). The peak at 721 cm^{-1} represents the rocking vibration of the CH_2 groups. The peaks at 580 and 450 cm^{-1} correspond to the stretching vibrations of the Ir-O and Ir-Cl bonds, respectively, indicating the coordination of the Ir atom with the O and Cl atoms (Nakamoto, 2009).

Table 2 compares key IR bands across complexes 1-6. The IR spectra are similar, with only minor shifts in ν(O-S-O) and ν(S-O) due to the changing alkyl chain length. The ν(O-S-O) and ν(S-O) bands, expectedly, (Nakamoto, 2009), shift to higher wavenumber with increasing chain length, indicating stronger S-O bonding upon coordination. Small increases in ν(Ir-O) and ν(Ir-Cl) follow the same trend. All six complexes show bands consistent with coordinated alkyl sulphate and chloride ligands. The systematic shift to higher wavenumber supports coordination of the sulphate group to Ir(V). The IR spectra of complexes 1–6 display characteristic bands for the coordinated alkyl sulphate and chloride ligands. Table 2 summarizes the key vibrations.

Table 2. Selected IR bands (cm^{-1}) for complexes 1–6

Complex	ν(O-S-O)	ν(S-O)	ν(Ir-O)	ν(Ir-Cl)
$[Ir(SDS)_2Cl_2]Cl$	1216	1066	576	450
$[Ir(Myristyl)_2Cl_2]Cl$	1218	1068	583	452
$[Ir(Cetyl)_2Cl_2]Cl$	1222	1072	584	453
$[Ir(Stearyl)_2Cl_2]Cl$	1223	1073	587	455
$[Ir(Arachidyl)_2Cl_2]Cl$	1224	1076	588	456
$[Ir(Behenyl)_2Cl_2]Cl$	1226	1078	592	458

The spectra of all six complexes are similar, confirming an identical coordination mode. Bands at 2924–2930 cm^{-1} and 2853–2859 cm^{-1} correspond to asymmetric and symmetric C–H stretching of the alkyl chains, while the band at ~1467 cm^{-1} is due to CH_2 bending.

The ν(O-S-O) and ν(S-O) bands shift to higher wavenumber with increasing chain length, from 1215 and 1068 cm^{-1} in complex 1 to 1225 and 1076 cm^{-1} in complex 6. This shift indicates a slight strengthening of the S–O bond upon coordination to Ir(V). Bands at 580–589 cm^{-1} and 450–458 cm^{-1} are assigned to ν(Ir-O) and ν(Ir-Cl), respectively. These also show a small increase with chain length, consistent with minor changes in the metal–ligand bond environment. Compared to the free sodium alkyl sulphates, the ν(O-S-O) and ν(S-O) bands shift to higher frequency in the complexes, confirming coordination of the sulphate group to the iridium centre through oxygen atoms. The pattern is consistent with bidentate binding in an octahedral geometry.

3.2 ^{1}H NMR Spectrum of $[Ir(SDS)_2Cl_2]Cl$

The ^{1}H NMR spectra of the complexes are shown below. For $[Ir(SDS)_2Cl_2]Cl$, the signals are assigned as follows: 0.83 (ppm) for the CH_3 (the terminal methyl group of the dodecyl chain) as a triplet, 1.25-1.40 (ppm) for the CH_2 (methylene groups in the dodecyl chain) as a multiplet, 1.60-1.70 (ppm) for the CH_2 (the methylene group adjacent to the oxygen atom in the dodecyl chain) as a multiplet, and 4.10 (ppm) for OCH_2 (the methylene group attached to the oxygen

atom in the dodecyl chain) as a triplet, along with 1.82 – 1.92 (ppm) (Silverstein *et al*., 2014). Unexpectedly, the proton NMR spectra of the complexes exhibit similar patterns, with the main differences being in the integration values of the methylene protons. The signals related to the alkyl sulphate ligands are assigned accordingly, confirming the presence of the alkyl.
The signals related to the alkyl sulphate ligands have been assigned, confirming their presence. The 1H NMR data for the complexes shows a strong indication that the ligands are bonding with the metal ions. The 1H NMR data for each complex are as follows:
Complex 1: $C_{24}H_{48}IrCl_3O_8S_2$: δ 0.84 (t, J = 6.4 Hz, 6H, CH_3); δ 1.20-1.36 (m, 32H, CH_2); δ 1.68 (m, 4H, CH_2); δ 3.42 (t, J = 5.5 Hz, 4H, OCH_2); δ 4.30 (m, 4H, OCH_2).
Complex 2: $C_{28}H_{60}IrCl_3O_8S_2$: δ 0.72 (t, J = 6.6 Hz, 6H, CH_3); δ 1.30-1.58 (m, 40H, CH_2); δ 1.58 (m, 4H, CH_2); δ 3.60 (t, J = 6.5 Hz, 4H, OCH_2); δ 4.20 (m, 4H, OCH_2).
Complex 3: $C_{32}H_{68}IrCl_3O_8S_2$: δ 0.75 (t, J = 6.8 Hz, 6H, CH_3); δ 1.30-1.40 (m, 48H, CH_2); δ 1.30 (m, 4H, CH_2); δ 3.40 (t, J = 6.5 Hz, 4H, OCH_2); δ 4.30 (m, 4H, OCH_2).
Complex 4: $C_{36}H_{76}IrCl_3O_8S_2$: δ 0.82 (t, J = 6.8 Hz, 6H, CH_3); δ 1.28-1.42 (m, 56H, CH_2); δ 1.62 (m, 4H, CH_2); δ 3.62 (t, J = 6.5 Hz, 4H, OCH_2); δ 4.32 (m, 4H, OCH_2).
Complex 5: $C_{40}H_{84}IrCl_3O_8S_2$: δ 0.84 (t, J = 6.8 Hz, 6H, CH_3); δ 1.26-1.42 (m, 64H, CH_2); δ 1.60 (m, 4H, CH_2); δ 3.50 (t, J = 6.5 Hz, 4H, OCH_2); δ 4.10 (m, 4H, OCH_2).
Complex 6: $C_{44}H_{92}IrCl_3O_8S_2$: δ 0.85 (t, J = 6.8 Hz, 6H, CH_3); δ 1.28-1.42 (m, 72H, CH_2); δ 1.62 (m, 4H, CH_2); δ 3.52 (t, J = 6.5 Hz, 4H, OCH_2); δ 4.20 (m, 4H, OCH_2).

3.3 Carbon 13-NMR Results

$[Ir(SDS)_2Cl_2]Cl$
The carbon 13-NMR spectrum for $[Ir(SDS)_2Cl_2]Cl$ displays signals at 14.5, 23.1-32.3, 69.1, and 71.5 ppm. The signal at 14.5 ppm is linked to the methyl carbon (CH_3) of the SDS ligand. The range of 23.1-32.3 ppm corresponds to the methylene carbons (CH_2) of the SDS ligand. Meanwhile, the signals at 69.1 and 71.5 ppm are associated with the methyleneoxy carbons (CH_2O) of the SDS ligand. When compared to the SDS ligand, these signals are slightly shifted downfield, indicating that the ligand is coordinating with the Ir ion (Silverstein *et al*., 2014).
For $[Ir(Myristyl\ sulphate)_2Cl_2]Cl$, the carbon 13-NMR spectrum reveals signals at 14.5, 23.1-32.3, 69.1, and 71.5 ppm. The signal at 14.5 ppm corresponds to the methyl carbon (CH_3) of the Myristyl sulphate ligand. The range of 23.1-32.3 ppm is attributed to the methylene carbons (CH_2) of the Myristyl sulphate ligand, while the signals at 69.1 and 71.5 ppm are linked to the methyleneoxy carbons (CH_2O) of the same ligand. Just like with the Myristyl sulphate ligand, there is a slight downfield shift in the signals, indicating that the ligand is coordinating with the Ir(V) centre.
The carbon 13-NMR spectrum of $[Ir(Cetyl\ sulphate)_2Cl_2]Cl$ shows similar signals at 14.5, 23.1-32.3, 69.1, and 71.5 ppm. Again, the 14.5 ppm signal is assigned to the methyl carbon (CH_3) of the Cetyl sulphate ligand, while the 23.1-32.3 ppm range corresponds to the methylene carbons (CH_2). The signals at 69.1 and 71.5 ppm are for the methyleneoxy carbons (CH_2O) of the Cetyl sulphate ligand. A downfield shift, indicating coordination with the Ir(V) centre was also shown.
For $[Ir(stearyl\ sulphate)_2Cl_2]Cl$, the carbon 13-NMR spectrum again shows signals at 14.5, 23.1-32.3, 69.1, and 71.5 ppm. The 14.5 ppm signal is linked to the methyl carbon (CH_3) of the stearyl sulphate ligand, while the 23.1-32.3 ppm range is for the methylene carbons (CH_2). The signals observed at 69.1 and 71.5 ppm correspond to the methyleneoxy carbons (CH_2O) found in the Stearyl sulphate ligand. When compared to the Stearyl sulphate ligand, these signals are slightly downfield, which suggests that the ligand is coordinating with the Ir(V) centre.
For the compound $[Ir(Arachidyl\ sulphate)_2Cl_2]Cl$, the carbon 13-NMR spectrum reveals signals at 14.5, 23.1-32.3, 69.1, and 71.5 ppm. The signal at 14.5 ppm is attributed to the methyl carbon

(CH_3) of the Arachidyl sulphate ligand, while the range of 23.1-32.3 ppm is assigned to the methylene carbons (CH_2) of the same ligand. The signals at 69.1 and 71.5 ppm are linked to the methyleneoxy carbons (CH_2O) of the Arachidyl sulphate ligand. Similar to the Arachidyl sulphate ligand, these signals are also slightly downfield, indicating that the ligand is coordinating with the Ir(V) centre.

The carbon 13-NMR spectrum of [Ir(Behenyl sulphate)$_2$Cl$_2$]Cl shows signals at 14.2, 23.2-32.3, 69.1, and 71.8 ppm as well. The 14.2 ppm signal is assigned to the methyl carbon (CH_3) of the Behenyl sulphate ligand, while the 23.2-32.3 ppm range corresponds to the methylene carbons (CH_2) of the Behenyl sulphate ligand. The signals at 69.1 and 71.8 ppm are for the methyleneoxy carbons (CH_2O) of the Behenyl sulphate ligand. Just like with the Behenyl sulphate ligand, these signals are slightly downfield, indicating coordination with the Ir(V) centre Overall, the carbon 13-NMR spectra of the Ir(V) complexes exhibit similar patterns to those of their respective ligands, with minor shifts in the chemical shifts likely due to the ligands coordinating with the Ir(V) centre.

The ^{13}C NMR spectrum reinforces the structural integrity of the dodecyl chain in [Ir(SDS)$_2$Cl$_2$]Cl. When examining the proton and carbon-13 NMR spectra of the Ir(V) complexes with various alkyl sulphate ligands, similar patterns were observed, which confirm the presence of these ligands. Interestingly, the proton and carbon-13 NMR spectra do not show significant variations as the alkyl chain length increases. They resemble those of other metal complexes featuring alkyl sulphate ligands. The signals associated with the alkyl sulfate ligands experience slight shifts, hinting at a potential influence of the Ir(V) centre on the ligand environment. Additionally, these signals are slightly broadened, suggesting a possible increase in the molecular weight of the complexes. The minor downfield shifts relative to free ligands confirm coordination to the Ir(V) centre. Table 3 further summarises both the ^{1}H and ^{13}C NMR results.

Table 3. ^{1}H and ^{13}C NMR chemical shifts for CH_3, CH_2, and OCH_2 groups in complexes 1–6

Chemical shift (ppm)						
	^{1}H nmr			^{13}C nmr		
	Group					
Complex	CH_3	CH_2	OCH_2*	CH_3	CH_2	OCH_2*
$[Ir(SDS)_2Cl_2]Cl$	0.84 (t, 6H)	1.20–1.36, 1.68 (m, 36H)	3.42 (t), 4.30 (m)	14.5	23.1–32.3	69.1, 71.5
$[Ir(Myristyl)_2Cl_2]Cl$	0.72 (t, 6H)	1.30–1.58, 1.58 (m, 44H)	3.60 (t), 4.20 (m)	14.5	23.1–32.3	69.1, 71.5
$[Ir(Cetyl)_2Cl_2]Cl$	0.75 (t, 6H)	1.30–1.40, 1.30 (m, 52H)	3.40 (t), 4.30 (m)	14.5	23.1–32.3	69.1, 71.5
$[Ir(Stearyl)_2Cl_2]Cl$	0.82 (t, 6H)	1.28–1.42, 1.62 (m, 60H)	3.62 (t), 4.32 (m)	14.5	23.1–32.3	69.1, 71.5
$[Ir(Arachidyl)_2Cl_2]Cl$	0.84 (t, 6H)	1.26–1.42, 1.60 (m, 68H)	3.50 (t), 4.10 (m)	14.5	23.1–32.3	69.1, 71.5
$[Ir(Behenyl)_2Cl_2]Cl$	0.85 (t, 6H)	1.28–1.42, 1.62 (m, 76H)	3.52 (t), 4.20 (m)	14.2	23.2–32.3	69.1, 71.8

**OCH_2 protons appear as two sets due to CH_2 adjacent to O and CH_2-O-SO_3 environments.*

The electronic transitions observed in the electronic transition studies are detailed in Table 4. The g-values (g∥ and g⊥) reflect the magnetic moment of the unpaired electron (Abragam & Bleaney, 1970). The axial symmetry hints at a tetragonal distortion of the octahedral geometry, probably because of the two chloride ligands present. Notably, the g∥ values are greater than the g⊥ values, which suggests that the octahedral geometry is compressed along the z-axis. As the alkyl chain length increases, the g∥ values decrease, indicating a reduction in tetragonal distortion. Conversely, the g⊥ values rise with longer alkyl chains, implying an increase in electron density at the Ir centre.

The electronic absorption spectra point to a low-spin d^5 configuration for the Ir(V) complexes. The ν_1 and ν_2 bands correspond to transitions from the ^2T2g ground state to the ^2Eg and ^2T1g excited states, respectively. The EPR spectra show axial symmetry, which aligns with the tetragonal distortion of the octahedral geometry (Figgis & Hitchman, 2000).

Table 4. Selected electronic absorption bands (cm^{-1}) of the ligands and their corresponding complexes

Compound	Electronic spectra Electronic band (cm^{-1}) ν_1 ν_2	Assignment	PR parameters g∥	g⊥
$C_{24}H_{48}Cl_3O_8S_2$	51,500	$\pi \rightarrow \pi^*$		
	40,600	$n \rightarrow n^*$		
$C_{24}H_{48}IrCl_3O_8S_2$	18,500	$^2T2g \rightarrow {}^2Eg$	2.45	2.10
	24,800	$^2T2g \rightarrow {}^2T1g$		
[Ir(Myristyl sulphate)$_2$Cl$_2$]Cl	18,300	$^2T2g \rightarrow {}^2Eg$	2.42	2.12
	24,600	$^2T2g \rightarrow {}^2T1g$		
[Ir(Cetyl sulphate)$_2$Cl$_2$]Cl	18,100	$^2T2g \rightarrow {}^2Eg$	2.40	2.13
	24,400	$^2T2g \rightarrow {}^2T1g$		
[Ir(Stearyl sulphate)$_2$Cl$_2$]Cl	17,900	$^2T2g \rightarrow {}^2Eg$	2.38	2.14
	24,200	$^2T2g \rightarrow {}^2T1g$		
[Ir(Arachidyl sulphate)$_2$Cl$_2$]Cl	17,700	$^2T2g \rightarrow {}^2Eg$	2.36	2.15
	24,000	$^2T2g \rightarrow {}^2T1g$		
[Ir(Behenyl sulphate)$_2$Cl$_2$]Cl	17,500	$^2T2g \rightarrow {}^2Eg$	2.34	2.16
	23,800	$^2T2g \rightarrow {}^2T1g$		

The mass spectrum of each of the complexes displayed mass-to-charge ratio (*m/z*) value as a single peak which correspond to their respective observed masses (M+1) value. (Gross, 2017). The fragmentation patterns of the six complexes are similar and straight forward. The molecular ions (M+) were 807.17 (calculated), 807.34 (found); 887.52 (calculated), 887.58(found); 943.63 (calculated), 943.54(found); 999.63 (calculated), 999.58 (found); 1055.93 (calculated), 1055.88 (found) and 1111.84(calculated), 1111.90 (found), for complexes 1, 2, 3, 4, 5 and 6, respectively. These were in good agreement with the calculated molecular mass of the complexes. The mass spectrophotometry fragmentation patterns and assignments of the peak ions for the Ir(V) complexes are summarized in the Table 5 below. All the six complexes revealed base peaks which are as a result of the loss of the outer-sphere chloride counterions which are outside their coordination spheres giving the $[M - Cl]^+$cation. The systematic increment of 56.34 between successive homologues reflects the sequential C_2H_4 extension of the alkyl chains and attests to the homologous nature of the series.

Another fragmentation peaks, at m/z 323.6/325.4, which is found in the spectral of all of them, are ascribed to retention of the $IrCl_2$ core upon complete dissociation of the sulphate ligands. The peaks at 589.6 and 727.8 in the spectral of dodecyl (C_{12}) derivative and behenyl (C_{22}) respectively, correspond to $[Ir(alkyl\ sulphate)Cl_2]^+$, arising from the loss of one alkyl sulphate ligand. The calculated monoisotopic masses, based on using the ^{193}Ir isotope and ^{35}Cl (75.77%), are in agreement with the experimentally observed m/z values, thereby confirming the integrity of the bis(alkyl sulphate)dichloroiridium(V) core. Summarily, the MS data confirmed the molecular formulae of the six complexes. The observed isotopic profiles are congruent with theoretical distributions based on $^{191}Ir/^{193}Ir$ and $^{35}Cl/^{37}Cl$, and the minor mass discrepancies are as a result of isotopic compositions. Other details are presented in Table 5.

Table 5. Mass spectral data of the complexes

Complex	Molecular Ion (M^+)	Fragmentation Patterns
$[Ir(SDS)_2Cl_2]Cl$	807.34	$[Ir(SDS)_2Cl_2]^+ \rightarrow [Ir(SDS)Cl_2]^+ + Cl^-$
$[Ir(Myristyl\ sulphate)_2Cl_2]Cl$	887.58	$[Ir(Myristyl\ sulphate)_2Cl_2]^+ \rightarrow [Ir(Myristyl\ sulphate)Cl]^+ + Cl^-$
$[Ir(Cetyl\ sulphate)_2Cl_2]Cl$	943.54	$[Ir(Cetyl\ sulphate)_2Cl_2]^+ \rightarrow [Ir(Cetyl\ sulphate)Cl]^+ + Cl^-$
$[Ir(Stearyl\ sulphate)_2Cl_2]Cl$	999.58	$[Ir(Stearyl\ sulphate)_2Cl_2]^+ \rightarrow [Ir(Stearyl\ sulphate)Cl]^+ + Cl^-$
$[Ir(Arachidyl\ sulphate)_2Cl_2]Cl$	1055.88	$[Ir(Arachidyl\ sulphate)_2Cl_2]^+ \rightarrow [Ir(Arachidyl\ sulphate)Cl]^+ + Cl^-$
$[Ir(Behenyl\ sulphate)_2Cl_2]Cl$	1111.90	$[Ir(Behenyl\ sulphate)_2Cl_2]^+ \rightarrow [Ir(Behenyl\ sulphate)Cl]^+ + Cl^-$

Based on the revelations from the spectrophotometric studies carried on the metal complexes, they are found to all have octahedral geometry (Lever, 1984). In each case, two chloride, two O atoms (highly electronegative) of the $-OSO_3^-$, of the alkyl sulphate group forming a bidentate coordination. are coordinated to the Ir ion. The structure of a representative complex, which is typical of all the complexes, is shown below. The mass spectrometry data confirms the molecular weights of the complexes (Gross, 2017).

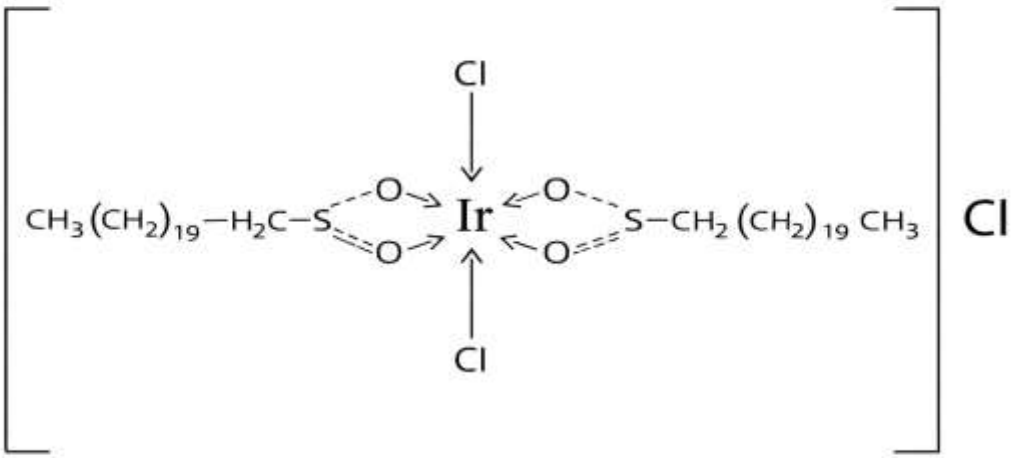

Figure 1. Proposed octahedral structure for $[Ir(R\text{-}OSO_3)_2Cl_2]Cl$ complexes (where R = C_{12}–C_2 alkyl chain. Two bidentate sulphate ligands occupy equatorial positions; chlorides occupy axial positions).

3.4 Thermal Stability and Phase Transitions of the Ir(V) Complexes.

Thermogravimetric analyses (TGA), under flow of nitrogen, were performed on all the samples to ascertain their thermal stability and decomposition behaviour (Brown, 2001). The DSC curves of the complexes are obtained at different temperatures (30-300 °C) at a heating rate of 10 °C/min (Höhne *et al*., 2003). The differential scanning calorimetry (DSC), differential thermal analysis DTA, and polarised optical microscopy (POM) show that mesogenic behaviour depends strongly on alkyl chain length (Bruce, 2000) and (Binnemans, 2005).

The DTA thermograms for all the complexes reveal clear endothermic and exothermic transitions that correspond to phase changes, including crystalline-to-mesophase (Cr → LC), mesophase-to-isotropic liquid (LC → Iso), and decomposition events (Demus *et al*., 1998). The complex with the shortest chain, $[Ir(SDS)_2Cl_2]Cl$, displays relatively weak and broad endothermic peaks, suggesting that the mesophase formation is not well-defined. This implies that shorter alkyl chains did not provide the strong intermolecular interactions needed for stable liquid crystalline ordering (Binnemans, 2005). Longer alkyl chains produce sharper, more intense endotherms. Melting points and mesophase stability increase because stronger van der Waals interactions improve molecular packing.

TGA shows no mass loss below 100 °C, confirming the absence of coordinated water. Decomposition occurs in three steps: loss of alkyl sulphate ligands, breakdown of the coordination sphere, and formation of Ir/IrO_2 residue. Decomposition temperatures rise from

253 °C for complex 1 to 305 °C for complex 6, reflecting the stabilizing effect of longer alkyl chains (Höhne *et al*., 2003).

Table 6: Melting Point and Decomposition Temperature of Complexes

Complex	Melting Point (°C)	Decomposition Temperature (°C)
1	118	253
2	130	258
3	136	274
4	153	282
5	160	290
6	171	305

The melting points and decomposition temperatures increase with increasing alkyl chain length.

The enthalpy changes, ΔH (kJ/mol), for the phase transitions for the complexes were found as: for complex 1, 51.60; for complex 2, 57.20; for complex 3, 62.55; for complex 4, 68.48; for complex 5, 73.24; for complex 6, 78.60 (Höhne *et al*., 2003). The entropy changes, ΔS (J/mol·K), for the phase transitions for the complexes were found as: for complex 1, 103; for complex 2, 114; for complex 3, 126; for complex 4, 135; for complex 5, 146; for complex 6, 154. The sequence showed that as the chain length increases, there is increase in the entropy change.

The Ir(V) complexes have higher thermal stability than the corresponding Cu(II) and Zn(II) complexes with alkyl sulphate ligands (Date *et al*., 2002; Neumann *et al*., 2010). These studies have revealed, significantly, the thermal properties of Ir(V) complexes, which is crucial for their potential applications in fields like catalysis, electronics, and medicine (Zhao *et al*., 2011). It also reveals that the thermal stability of these complexes is affected by the length of the alkyl chain in the sulphate ligand, offering a fresh perspective on designing thermally stable Ir(V) complexes. The liquid crystalline behaviours of the six new complexes were investigated using differential thermal analysis (DTA) and thermogrametric analysis. In general, the results revealed a strong dependence of liquid crystalline behaviours on the alkyl chain length of the coordinated sulphate ligands.

The DTA thermograms for all the complexes reveal clear endothermic and exothermic transitions that correspond to phase changes, including crystalline-to-mesophase (Cr → LC), mesophase-to-isotropic liquid (LC → Iso), and decomposition events. The complex with the shortest chain, $[Ir(SDS)_2Cl_2]Cl$, displays relatively weak and broad endothermic peaks, suggesting that the mesophase formation is not well-defined. This implies that shorter alkyl chains did not provide the strong intermolecular interactions needed for stable liquid crystalline ordering. Sharper and more intense endothermic peaks were observed as the alkyl chain lengths increases. The transition temperatures and stability of the mesophase increase with increase in chain length due to the presence of enhanced van der Waals iinteractions between longer hydrocarbon chains which is known to promote better molecular packing and stabilization of ordered mesophases.

From the TGA studies, none of the complexes showed weight loss below 100 ^{o}C. This indicates lack of lattice or coordinated water molecules in the complexes. Three main decomposition stages occurred at higher temperatures in all the complexes: The first stage involves the loss of alkyl sulphate ligands, the second stage was the breakdown of the coordination sphere, while, the last step was the formation of the final residue: metallic iridium or iridium oxide. The trends of the thermal stabilities of the complexes increase with increase of alkyl chain length. These trends reflect stronger intermolecular interaction and increased molecular weight which enhance resistance to thermal decomposition.

The mesophase can be found across a broad temperature range in longer-chain complexes before they start to break down. In contrast, complexes with short-chain ligands displayed only

limited mesomorphic behaviour, while those with longer chains showed well-defined and thermally stable mesophases, mainly of the smectic type. The findings highlighted how the design of molecular weight in metallomesogen systems can lead to significant differences in mesophase formation, stability, and thermal behaviour due to variations in ligand structures (Binnemans, 2005). There are strong signs that long-chain iridium complexes could be excellent materials for use in fields like optoelectronics, molecular organization, and functional soft materials (Zhao *et al*., 2011; Fan *et al*., 2018).

The tunable melting points (118–171 °C) and decomposition temperatures (253–305 °C) suggest these complexes are suitable for processing into thin films for OLED and sensor applications. Longer-chain complexes form stable smectic phases up to 250 °C, making them candidates for thermally robust liquid crystal displays and molecular ordering layers. Future work will explore thin-film deposition and charge transport properties.

4.0 Conclusion

Six novel iridium(V) complexes containing long-chain alkyl sulphate chloride ligands were successfully synthesized and characterized using FTIR, NMR, mass spectrometry, electronic spectroscopy, conductivity, magnetic susceptibility, and thermal analyses. The results confirmed successful coordination of the ligands to the Ir(V) centre and established a low-spin d^5 electronic configuration. Conductivity measurements indicated that all the complexes exhibit 1:1 electrolyte behaviour, confirming their ionic nature in solution. Thermal analysis showed that increasing the alkyl chain length enhanced the melting point, decomposition temperature, and liquid crystalline behaviour, demonstrating improved thermal stability. These findings reveal that the physicochemical properties of the complexes can be effectively tailored by varying the alkyl chain length. The combination of thermal stability, ionic conductivity, and structural integrity suggests that these complexes possess significant potential for applications in catalysis, optoelectronics, and advanced functional materials. Further studies on their electrochemical, catalytic, and photophysical properties are recommended to fully explore their technological and industrial potential.

References

1. Abragam, A. and Bleaney, B. (1970). Electron paramagnetic resonance of transition ions. Oxford University Press.
2. Armarego, W. L. F. (2017). Purification of laboratory chemicals (8th ed.). Butterworth-Heinemann.
3. Binnemans, K. (2005). Ionic liquid crystals. Chemical Reviews, 105(11), 4148–4204. https://doi.org/10.1021/cr0400919
4. Binnemans, K. (2009). Luminescence of metallomesogens. Journal of Materials Chemistry, 19(4), 448–459. https://doi.org/10.1039/b811373f
5. Brown, M. E. (2001). Introduction to thermal analysis: Techniques and applications (2nd ed.). Kluwer Academic.
6. Bruce, D. W. (2000). Calamitic metallomesogens. In D. W. Bruce, R. Walton and D. O'Hare (Eds.), Inorganic materials (2nd ed., pp. 429–462). Wiley.
7. Crabtree, R. H. (2019). The organometallic chemistry of the transition metals (7th ed.). Wiley.
8. Date, R. W., Iglesias, E. F., Rowe, K. E., Elliott, J. M. and Bruce, D. W. (2002). Metallomesogens by ligand design. Dalton Transactions, 2002(10), 1914–1931. https://doi.org/10.1039/b204543p
9. Date, R. W., Iglesias, E. F., Rowe, K. E., Elliott, J. M. andBruce, D. W. (2025). Metallomesogens by ligand design. Dalton Transactions, 2025(10), 1914–1931. https://doi.org/10.1039/b204543p

10. Demus, D., Goodby, J., Gray, G. W., Spiess, H. W. and Vill, V. (1998). Handbook of liquid crystals_ (Vol. 1). Wiley-VCH.
11. Dierking, I. (2003). Textures of liquid crystals. Wiley-VCH.
12. Donni, N. B., Guillon, D., Deschenaux, R. and Bruce, D. W. (2003). Metallomesogens. In J. A. McCleverty & T. J. Meyer (Eds.), Comprehensive coordination chemistry II (Vol. 7, pp. 357–627). Elsevier.
13. Earnshaw, A. (1968). Introduction to magnetochemistry. Academic Press.
14. Fadeeva, V. P., Tikhova, V. D. and Nikulicheva, O. N. (2008). Elemental analysis of organic compounds with the use of automated CHNS analyzers. Journal of Analytical Chemistry, 63(11), 1094–1106. https://doi.org/10.1134/s1061934808110142
15. Fan, C., Yang, C. and You, Y. (2018). Iridium(III) complexes for bioimaging. Coordination Chemistry Reviews, 374, 204–236. https://doi.org/10.1016/j.ccr.2018.07.003
16. Figgis, B. N., & Hitchman, M. A. (2000). Ligand field theory and its applications. Wiley-VCH.
17. Geary, W. J. (1971). The use of conductivity measurements in organic solvents for the characterisation of coordination compounds. Coordination Chemistry Reviews, 7(1), 81–122. https://doi.org/10.1016/s0010-8545(00)80009-0
18. Giroud-Godquin, A. M. and Maitlis, P. M. (1991). Metallomesogens: Metal complexes in organized fluid phases. Angewandte Chemie International Edition, 30(4), 375–402. https://doi.org/10.1002/anie.199103751
19. Gross, J. H. (2017). Mass spectrometry: A textbook (3rd ed.). Springer. https://doi.org/10.1007/978-3-319-54398-7
20. Höhne, G. W. H., Hemminger, W. F. and Flammersheim, H. J. (2003). Differential scanning calorimetry (2nd ed.). Springer. https://doi.org/10.1007/978-3-662-06710-9
21. Housecroft, C. E. and Sharpe, A. G. (2018). Inorganic chemistry (5th ed.). Pearson.
22. Lever, A. B. P. (1984). Inorganic electronic spectroscopy (2nd ed.). Elsevier.
23. Lowry, M. S., & Bernhard, S. (2006). Synthetically tailored excited states: Phosphorescent, cyclometalated iridium(III) complexes and their applications. Chemistry: A European Journal, 12(31), 7970–7977. https://doi.org/10.1002/chem.200600618
24. Nakamoto, K. (2009). Infrared and Raman spectra of inorganic and coordination compounds (6th ed.). Wiley.
25. Neumann, T., Dienes, Y., and Baumgartner, T. (2010). Luminescent metallomesogens. Dalton Transactions, 39(39), 9115–9130. https://doi.org/10.1039/c0dt00162h
26. Rosen, M. J., & Kunjappu, J. T. (2012). Surfactants and interfacial phenomena (4th ed.). Wiley.
27. Shriver, D. F., & Atkins, P. W. (2010). Inorganic chemistry (5th ed.). W. H. Freeman.
28. Silverstein, R. M., Webster, F. X., Kiemle, D. J., and Bryce, D. L. (2014). _Spectrometric identification of organic compounds (8th ed.). Wiley.
29. You, Y., & Nam, W. (2012). Photofunctional triplet excited states of cyclometalated Ir(III) complexes: Beyond electroluminescence. Chemical Society Reviews, 41(21), 7061–7084. https://doi.org/10.1039/c2cs35171d
30. Zhao, Q., Li, F., and Huang, C. (2011). Phosphorescent chemosensors based on heavy-metal complexes. Chemical Society Reviews, 40(8), 3007–3030. https://doi.org/10.1039/b926190a